Research Article

MWCNTs attached neodymium doped-ZnO photocatalysts for efficient removal of dyes from wastewater

William Wilson Anku[1] · Eric Selorm Agorku[2] · Samuel Osei-Bonsu Oppong[3] · Anthony Yaw Karikari[1]

Abstract
The present study involves the synthesis of neodymium-doped zinc oxide nanoparticles decked multiwalled carbon nanotubes (Nd-ZnO-MWCNTs) with different weight percentage compositions of Nd through the co-precipitation method. The synthesized photocatalysts were utilized in photocatalytic removal of acid blue 40 and eosin Y dye solutions via visible light irradiation. The influence of catalyst dose and dye concentrations on the degradation efficiency was also studied. The catalysts were characterized using XRD, FTIR, BET surface area analysis, UV–Vis and TEM spectroscopies. TEM revealed that the Nd-ZnO nanoparticles were well distributed on the MWCNTs surface. XRD analysis showed that the ZnO occurred in the wurtzite phase. The introduction of Nd and MWCNTs reduced the band gap of ZnO from 3.2 to 2.7 eV resulting in its enhanced visible light absorption. All the modified ZnO photocatalysts degraded the dye at higher efficiencies compared to the bare ZnO with 0.6% Nd-ZnO-MWCNTs being the most effective. The bare ZnO degraded 13% of acid blue 40 dye while 0.6% Nd-ZnO-MWCNTs exhibited 99% degradation efficiency. The synergistic effect of Nd and MWCNTs was identified to be responsible for the enhanced efficiency of the Nd-ZnO-MWCNTs photocatalysts.

Keywords ZnO · Photocatalytic degradation · Dyes · Visible light irradiation · Metal doping · Multiwalled carbon nanotubes

1 Introduction

The scarcity of clean and safe water is a global challenge that the world is faced with. With water being an essential commodity for all living organisms and the running of industries, we are faced with the challenge of having to provide clean water while making sure our reservoirs do not run dry [1]. Water pollution continues to be a foremost concern because efforts being put in place to provide safe water are struggling to meet the ever-increasing demand. This situation is worsened by the global climate change, continuous deterioration of water quality, and population growth [2]. Meanwhile, there continue to be enormous volumes of wastewater pumped directly into streams, rivers, and the ocean throughout the world.

The textile industry is known to contribute significantly to water pollution across the world [3] and organic dyes are major sources of environmental contaminants in water. These dyes mainly originate from textile industries during the processing of fibers and fabrics [4]. Wastewater effluents containing dyes have an intense color that requires treatment before their final discharge into the mainstream water bodies. It has been reported that textile and paper industries utilize large quantities of dyes which are known to cause serious hazards to humans and aquatic organisms [5]. When these toxic pollutants are discharged in the streams, they cause a drastic decrease in oxygen

concentration as they interfere with sunlight penetration through the water body which therefore becomes harmful to the ecosystem, particularly photosynthetic organisms [5]. The implications of water pollution on human health are severe aside from the effects on fish and other aquatic organisms.

Many conventional methods of wastewater treatment such as coagulation, adsorption, filtration, etc. have been tested for their abilities to remove these pollutants but are considered to be inefficient in the purification/treatment of wastewater [6–8]. Photocatalysis, a nanotechnology-based photochemical process, is providing a cheap solution to wastewater treatment without the need for bulky infrastructure or a centralized system. Photocatalytic degradation method can remove water pollutants with the use of metal oxide semiconductors and solar light with minimum waste and no secondary waste generation [9].

Metal oxide semiconductor photocatalysts such as ZnS, ZrO_2, SiO_2, ZrO_2, TiO_2, etc. possess the ability to degrade complex organic dyes in water. Consequently, they are being explored to perform important roles in wastewater treatment [8, 9]. Zinc oxide (ZnO) has been widely studied as a photocatalyst because of its special properties such as high crystalline structure, phase stability, excellent optical and mechanical properties which are required of a good photocatalyst [10]. However, the efficiency of ZnO as a photocatalyst for the degradation of dyes in water is affected by certain problems. These problems include its low tendency to efficiently utilize solar energy due to its wide band gap, small surface area, and high rate of recombination of photogenerated electrons and holes.

One approach that can be used to overcome these problems is the doping of ZnO with metals. Metal dopants are noted to augment the photocatalytic degradation tendencies of semiconductor photocatalysts. Doping of semiconductors with Lanthanide ions has been identified to minimise the rate of recombination of charge carries though the creation of charge carrier space regions on the metal oxide or entrapment of the excited electrons [11]. Metal dopants are also known to decrease the band gap of metal oxides with the subsequent improvement in their visible light utilization [12, 13] which is a requirement for an efficient photocatalytic activity. For example, neodymium (Nd) doping of TiO_2 has been recognised as a feasible technique for augmenting its photocatalytic activity where the Nd acts as an electron sink and thus prevented the rate at which the generated electrons and holes recombine. It was also noted to decrease the band gap of TiO_2 leading to an improvement in its organic pollutant removal efficiency in the visible region of the solar spectrum [14].

Some semiconductors photocatalysts have also been modified with multiwalled carbon nanotubes (MWCNTs)

so as to establish the probable application of MWCNTs-based nanocomposites in organic dyes removal in water [15–17]. MWCNT has unique properties that enable it to be used as a support for attachment of nanoparticles for use in water treatment. These properties include good charge carrier distribution and release mechanism, large surface area and hence high adsorption properties. It also has the ability to act as a photosensitizer [18] thereby improving the solar energy conversion efficiency of the resultant photocatalyst. A photocatalyst consisting of ZnO, Nd and MWCNTs is therefore projected to be effective against the removal of organic pollutants in wastewater.

In this work, we synthesized Nd-doped ZnO nanoparticles with varied Nd weight percentage concentrations and attached them onto functionalized MWCNTs (f-MWCNTs) to form Nd-ZnO-MWCNTs nanocomposites. This is projected to increase the surface area of ZnO, reduce its band gap and hence improve its visible light absorption ability so as to enhance its photocatalytic degradation tendency. The photocatalytic degradation ability of the catalysts was determined by using them to degrade acid blue 40 and eosin Y dyes in water under visible light exposure.

2 Experimental

2.1 Materials

The materials used to prepare the MWCNT-Nd-ZnO composites are as follow: Polyethylene glycol (PEG), Zinc acetate dihydrate [$Zn(CH_3COO)_2 \cdot 2H_2O$], nitric acid ($HNO_3$), 55%, sodium hydroxide (NaOH) neodymium nitrate hexahydrate ($Nd(NO_3)_3 \cdot 6H_2O$), acid blue 40 and eosin Y dyes. These chemicals were all procured from Sigma-Aldrich. Multiwalled carbon nanotube (MWCNTs) with purity > 95% was procured from Bayer Material Science AG in Germany. All the reagents were used as received with no purification. Preparation of the dyes stock solutions was achieved through the dissolution of their appropriate masses in 1000 mL of deionized water. The desired concentrations of the dye solutions (20 ppm) were prepared by dilution of the stock solutions.

2.2 MWCNTs functionalization

The MWCNTs were functionalized in order to ensure the attachment of the nanoparticles onto their surfaces. The first step in the MWCNTs functionalization was their dispersion in 55% HNO_3 through ultrasonication at 30 °C for 30 min. The dispersed MWCNTs were then taken through refluxing for 5 h at 100 °C in a closed system while being stirred constantly with a magnetic stirrer. The mixture was cooled and filtered using deionized water

and polytetrafluoroethylene (PTFE, 0.2 μm) membrane. The functionalized MWCNTs (f-MWCNTs) were then taken through copious washing until the pH was reduced to around 7. They were then oven-dried for 24 h at 100 °C and cooled to room temperature.

2.3 Preparation of Nd-ZnO-MWCNTs nanocomposites

The synthesis of Nd-ZnO-MWCNTs nanocomposites with 1: 0.04 ratio (ZnO: MWCNTs) and different weight percent Nd dopant concentrations (0.3%, 0.6%, 1.0%, and 2.0%) was achieved through the homogenous co-precipitation method. The functionalized MWCNTs (0.4 g) were suspended in 100 mL deionized water in a beaker through ultrasonication for 1 h. Calculated masses of Nd $(NO_3)_3 \cdot 6H_2O$ (depending on the percentage doping of Nd) and 10 g of Zn $(CH_3COO)_2 \cdot 2H_2O$ were also dissolved in deionized water (100 mL) in a separate beaker. These solutions were also taken through 30 min of sonication and another 30 min magnetic stirring to ensure uniform suspension. The two solutions were then mixed and stirred for 45 min. Approximately 2 mL of PEG was added to the suspension under continuous magnetic stirring after which NaOH solution (0.3 M) was added dropwise to precipitate the Nd-ZnO-MWCNTs Nanocomposites at around pH 9. The system was stirred for an additional 1 h, filtered, washed copiously with ethanol-deionized water mixture followed by drying at 100 °C for 12 h. Calcination of the samples was later performed at 400 °C for 3 h followed by pulverization. The unmodified ZnO and the ZnO-MWCNTs were also synthesized using the same produced but without the addition of the dopant precursor.

2.4 Samples characterization

Philips PANalytical X'pert PRO X-ray diffractometer was used to characterize the phase, crystallinity, and sizes of the bare and modified ZnO based samples. It was operated at 40 kV using Cu-Kα radiation (λ = 0.15406 nm) over a diffraction angle range of 2θ = 10°–80°. By using Deby–Scherrer's equation (Eq. 1) [19], the particle sizes were calculated.

$$D = \frac{K_\lambda}{\beta \cos \theta} \tag{1}$$

In this equation, D represents the crystallite size while K, which has a value of 0.9, is the shape factor. λ with a value of 0.15406 nm denotes the wavelength of the X-ray while β represents the full width at half maximum (FWHM) in 2θ scale, with θ being the Bragg's diffraction angle at the maximum.

PerkinElmer spectrometer (Spectrum 100) was used to record the FTIR of the samples in a 400–4000 cm^{-1} wavelength range using a KBr pellet. SEM on TESCAN (Vega 3 XMU) was used to analyse the surface morphology of the pristine and modified ZnO nanocomposites. For the internal morphology and size analyses, TEM (JEOL, JEM-2100F, 120 kV) was used while the optical absorptivity of the samples was determined with the help of a Shimadzu UV-2450 UV–Vis spectrophotometer.

2.5 Photocatalytic ability assessments

The tendency of the synthesized ZnO, ZnO-MWCNTs, and the Nd-ZnO-MWCNTs nanocomposites to degrade toxic organic pollutants in water was tested by applying them in the degradation of two different textile dyes (acid blue 40 and eosin Y dyes) by irradiation with visible light. This was achieved through the dispersion of 0.2 g of the photocatalysts (ZnO, ZnO-MWCNTs, 0.3% Nd-ZnO-MWCNTs, 0.6% Nd-ZnO-MWCNTs, 1.0% Nd-ZnO-MWCNTs, and 2% Nd-ZnO-MWCNTs) in 200 mL of 20 mg/L concentrations of the acid blue 40 and eosin Y dyes. At the initial stage, the dye-catalyst mixtures were stirred without light exposure for 30 min with a magnetic stirrer so as to create adsorption equilibrium between the catalysts and the dye molecules. Thereafter, the system was exposed to visible light produced by a full spectrum solar simulator (Port 9600) furnished with a 150 W ozone free xenon lamp which was fitted with a 420 nm dichroic UV filter. The mixtures were then stirred magnetically upon light exposure at room temperature for 3 h. During this 3 h, 5 mL aliquots of the irradiated dye solutions were withdrawn at 30 min intervals using 0.45 μm PVDF membrane fitted disposable syringes. The dyes' concentrations in each of the withdrawn solutions were determined with a Shimadzu spectrophotometer (UV-2450).
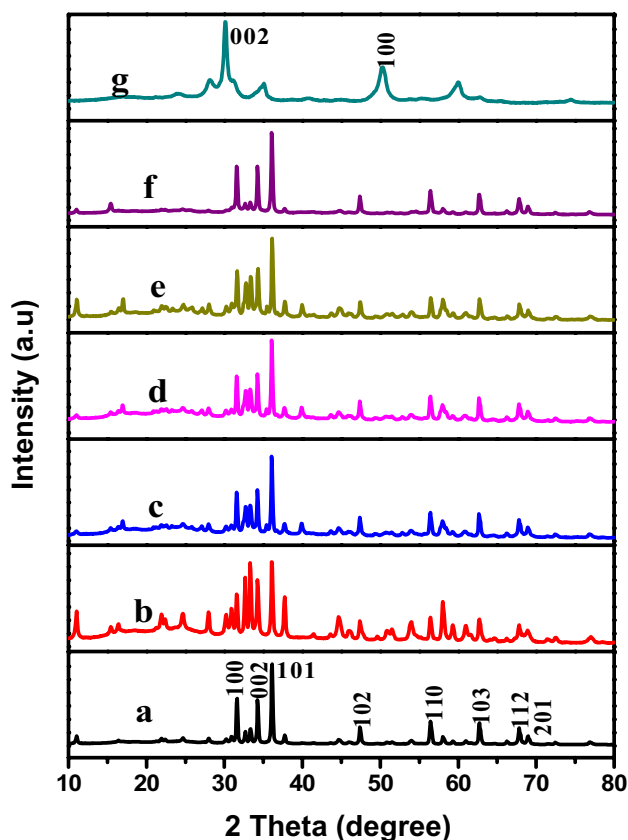
2.6 Effect of dye concentration and catalyst dose on degradation efficiency

For the influence of catalyst dose, different masses of the catalyst ranging from 0.1 to 0.7 g/L were used to degrade 100 mL of 20 mg/L dye solution. With regards to the influence of dye concentration, different concentrations of the dye in the range of 5–60 mg/L were degraded using the optimised catalyst dose. In both cases, the degradation experiment followed the same procedure as described in Sect. 2.5 for 180 min.

3 Results and discussions

3.1 XRD analysis

The XRD patterns of the photocatalysts (ZnO, ZnO-MWC-NTs and Nd-doped ZnO-MWCNTS photocatalysts), and the f-MWCNTs are presented in Fig. 1. In Fig. 1a which represents the XRD pattern of ZnO, the diffraction peaks at 31.93°, 34.57°, 36.43°, 47.57°, 56.75°, 62.95°, 68.11° and 69.35° correspond to (100), (002), (101), (102), (110), (103), (112) and (201) crystalline planes of ZnO, respectively. These indexed planes of the nanoparticles indicate that the ZnO occurs in the wurtzite structure based on JCPDS standard card number 01–075-0576 of ZnO [20]. Figure 1g represents the XRD pattern of the f-MWCNTs. The diffraction peaks of the f-MWCNTs occurring at $2\theta = 30.1°$ and 50.3° represent (002) and (100) diffractions of hexagonal graphite structure for MWCNTs. The intensities of these peaks in the spectra of ZnO-MWCNT and the series of Nd-ZnO-MWCNT (Fig. 1b–f) are very low due to the low content of MWCNTs in the samples (ZnO: MWCNTs, 1: 0.04).
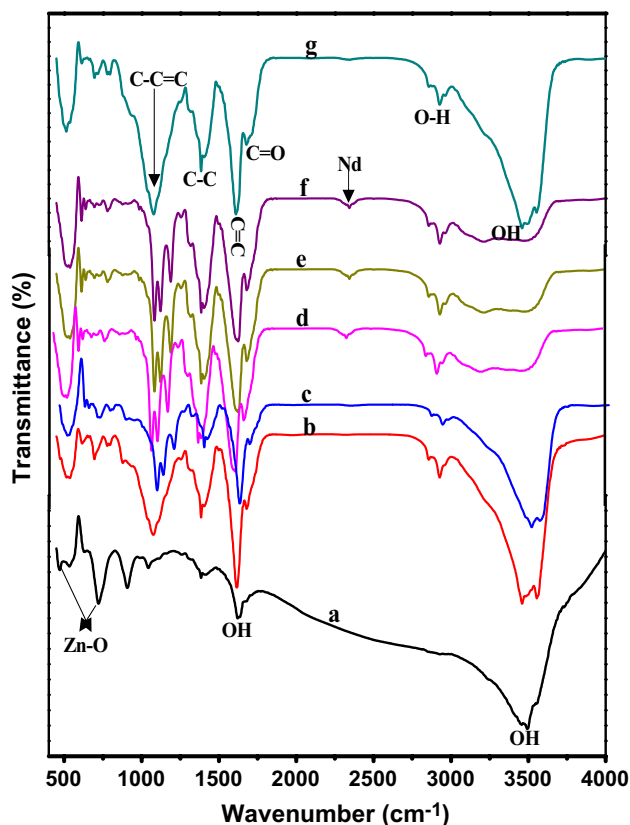
The crystalline sizes of the samples were calculated using the Debye–Shrerres equation as indicated in Eq. 1. The average crystalline size of the samples was calculated to be between 34 and 65 nm.

3.2 FTIR analysis

Figure 2 depicts the FTIR spectra of the ZnO, ZnO-MWC-NTs and Nd-ZnO-MWCNTs composites with different Nd concentrations. For all the samples, the broad peak located between 3000 cm^{-1} and 4000 cm^{-1} is assigned to –OH stretching vibration as a result of water molecules adsorbed on the surface of the nanoparticles. Figure 2a represents the FTIR spectrum of the unmodified ZnO. The peaks of this spectrum between 500 and 1000 cm^{-1} represent the Zn–O bonds vibrations. The peak situated at 1630 cm^{-1} is attributed to –OH bending vibration owing to water molecules adsorbed on the surface of the nanoparticles. The spectrum of the functionalized MWCNTs is presented in Fig. 2g. Again, the broad and sharp peak between 3000 and 4000 cm^{-1} is indicative of –OH groups associated with water molecules adsorbed on the surface of the functionalized MWCNTs [21] while that between

Fig. 1 XRD spectra of (**a**) ZnO, (**b**) ZnO-MWCNTs, (**c**) 0.3% Nd-ZnO-MWCNTs, (**d**) 0.6% Nd-ZnO-MWCNTs, (**e**) 1.0% Nd-ZnO-MWCNTs, (**f**) 2% Nd-ZnO-MWCNTs and (**g**) functionalized MWCNTs

Fig. 2 FTIR spectra of (**a**) ZnO, (**b**) ZnO-MWCNTs, (**c**) 0.3% Nd-ZnO-MWCNTs, (**d**) 0.6% Nd-ZnO-MWCNTs, (**e**) 1.0% Nd-ZnO-MWCNTs and (**f**) 2% Nd-ZnO-MWCNTs
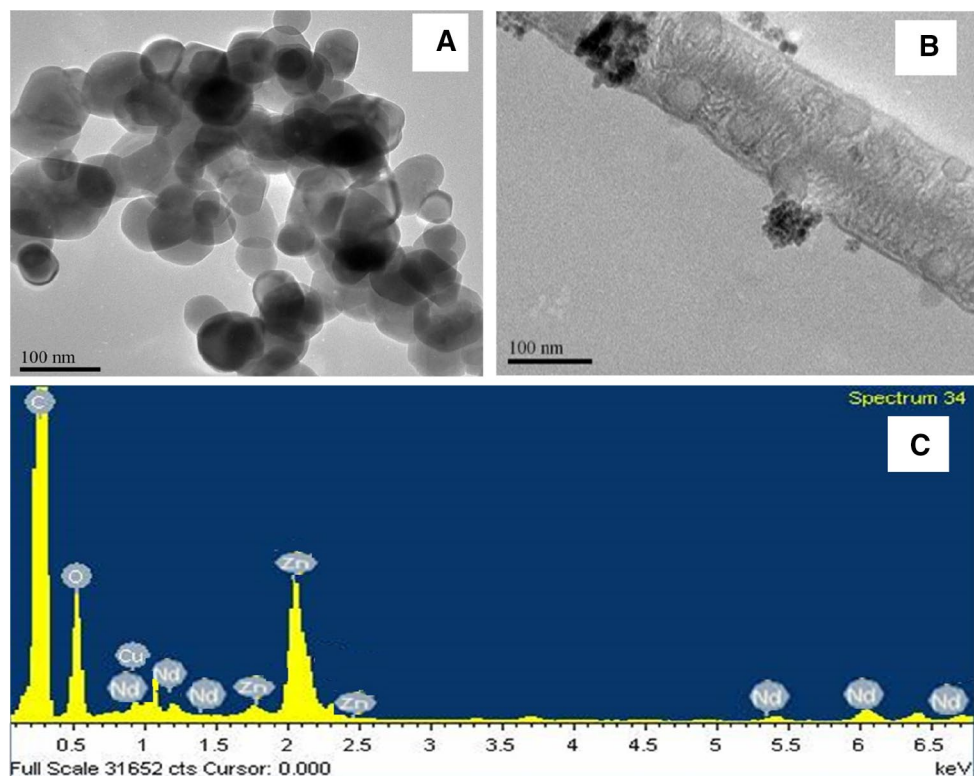
2750 and 3000 cm^{-1} signifies O–H stretching vibration. The C–C skeletal vibration and C=C bond stretching vibration of the MWCNTs are represented by the peaks around 1300 cm^{-1} and 1669 cm^{-1} respectively. The band between 1000 and 1300 cm^{-1} is accredited to C–C=C asymmetric stretching while the one at 1750 cm^{-1} indicates C=O stretching vibrations of the MWCNTs. The occurrence of these bands is indicative of the fact that the MWCNTs were successfully functionalized with a carboxylic acid group due to oxidation of some of the carbon atoms of the MWCNTs.

The spectra of all the other samples (ZnO-MWCNTs and Nd-ZnO-MWCNTs composites with different Nd concentrations) which are represented in Fig. 2b–f contain the peaks of both ZnO and MWCNTs. The difference in peak intensities of the bare ZnO and MWCNTs modified ZnO composites proves the interaction between the MWCNTs and the Nd-ZnO. A new peak emerges at 2340 cm^{-1} in the spectra of the Nd-ZnO-MWCNTs samples (Fig. 2c–f). This peak becomes more pronounced in the 0.6%, 1.0%, and 0.2% Nd-ZnO-MWCNTs samples and it is assigned to the presence of Nd dopant.

3.3 TEM analysis

Figure 3a–c represent the TEM image of the bare ZnO, TEM image of 0.6% Nd-ZnO-MWCNTs composite, and EDX spectrum of 0.6% Nd-ZnO-MWCNTs composite respectively.

According to Fig. 3a, the ZnO nanoparticles are spherical and possess regular/uniform size and morphology. In Fig. 3b, the surface of the MWCNTs is visibly and uniformly modified with Nd-ZnO nanoparticles. This uniform distribution of the ZnO nanoparticles is due to the functionalization of the MWCNTs with reactive carboxylic acid groups which enhanced the nanoparticle attachment onto the MWCNTs. The TEM result validates that of the XRD as the particle size obtained from TEM is also between 34 and 65 nm. Figure 3c represents the elemental conmposition of the catalyst which was determined through EDX analysis. The figure contains the expected elements (Zn, Nd, C and O) as the main components of the nanocomposite. The presence of these elements further confirms the successful synthesis of the Nd-ZnO-MWCNTs composite.

3.4 BET surface area analysis

BET surface area analysis was performed to provide specific surface area evaluation of the nanoparticles. Nitrogen adsorption–desorption isotherm was used to determine the BET surface area, pore volume and pore size of the catalysts (Table 1). The results show that the surface area of ZnO was low compared to the ZnO-MWCNTs composite, which further increased for the Nd-doped ZnO-MWCNTs. This suggests that the MWCNTS combined with ZnO, and incorporation of Nd in the ZnO-MWCNTs was successful. The results indicated that the surface area, pore size and

Fig. 3 TEM images of **a** ZnO, **b** 0.6% Nd-ZnO-MWCNTs composite, and **c** EDX spectrum of 0.6% Nd-ZnO-MWCNTs composite

Table 1 BET surface area, pore-volume, pore size, band gap, and percentage degradation after exposure to simulated solar light

Sample	BET surface area (m^2/g)	Pore volume (cm^3/g)	Pore size (Å)
ZnO	28.7012	0.1144	49.9322
ZnO-MWCNTs	36.5813	0.09578	40.4683
0.3% Nd-ZnO-MWCNTs	47.5432	0.2108	42.5564
0.6% Ce-ZnO-MWCNTs	47.4898	0.26464	39.3544
1.0% Ce-ZnO-MWCNTs	48.6480	0.3442	32.4785
2.0% Ce-ZnO-MWCNTs	47.4457	0.30762	36.0477
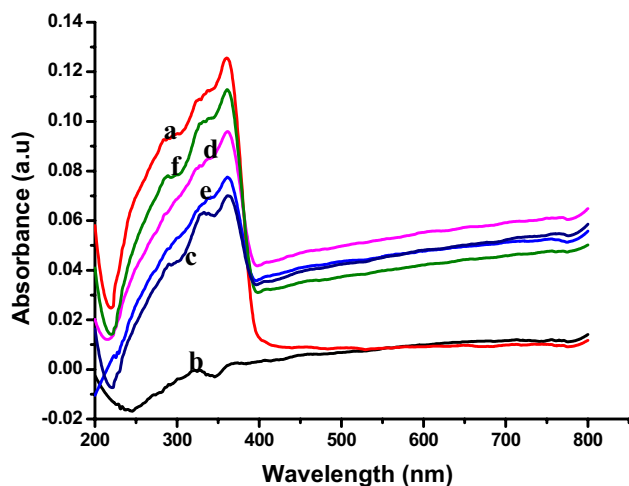
Fig. 4 UV–Vis spectra of (**a**) ZnO, (**b**) ZnO-MWCNTs, (**c**) 0.3% Nd-ZnO-MWCNTs, (**d**) 0.6% Nd-ZnO-MWCNTs, (**e**) 1.0% Nd-ZnO-MWCNTs and (**f**) 2% Nd-ZnO-MWCNTs

pore volume of the samples were independent on Nd concentration in ZnO-MWCNTS host material. The surface area of the Nd-ZnO-MWCNTs varied from 47.4457 to 48.6480 m^2/g.

3.5 Optical activity analysis

The optical activities of the photocatalysts were assessed with UV–Vis absorption spectroscopy. The absorbance spectra of the samples are presented in Fig. 4. According to Fig. 4, ZnO displayed the highest light absorption in the UV region (200–400 nm). However, upon the introduction of MWCNTs and Nd, the UV activity of ZnO reduced while its visible light activity increased as indicated in the modified ZnO samples (Fig. 4b–f). Thus, all the modified ZnO samples absorb light in the visible region (400–800 nm) with a significant increase in the visible light activity upon the introduction of Nd. ZnO-MWCNTs has comparatively small absorption in the visible region due to the very low content of MWCNTs in the samples (ZnO: MWCNTs, 1: 0.04).

It is worthy to note that the highest visible light activity was displayed by 0.6% Nd-ZnO-MWCNTs sample. Samples with Nd concentration greater than 0.6% (i.e. 1.0% Nd-ZnO-MWCNTs and 2.0% Nd-ZnO-MWCNTs) exhibited lower visible light absorptivity compared to 0.6% Nd-ZnO-MWCNTs and the absorptivity decreased with increasing Nd concentration. This observation suggests that the optimum Nd concentration for efficient visible light utilization of ZnO is 0.6%. Beyond optimum dopant concentration, metal ions act as recombination centers for both electrons and holes which affects the photoactivity of the catalyst [13]. High visible light absorptivity is known to result in corresponding higher photocatalytic activity [22], hence 0.6% Nd-ZnO-MWCNTs is anticipated to demonstrate the highest photocatalytic activity.

The band gaps of the photocatalysts were calculated using Kubelka–Munk equation (Eq. 2) which permits the optical absorbance of the samples to be approximated from their standard reflectance spectra. The obtained Kubelka–Munk function (F(R)) was plotted against wavelength based on Eq. 2:

$$F(R) = \frac{(1-R)}{2R} \qquad (2)$$

where R is the reflectance and it is designated as $(R) = R_{sample}/R_{reference}$. The plot of this analysis is shown in Fig. 5 and the band gaps of all the catalysts are presented in Table 1. The band gap of the bare ZnO obtained in this study (3.20 eV) is consistent with other published works [23]. The result revealed that ZnO experienced band gap reduction with the introduction of f-MWCNTs, and a further consistent reduction in band gap with increasing Nd concentration up to 0.6% Nd (the optimum dopant concentration). 1.0% Nd-ZnO-MWCNTs and 2.0% Nd-ZnO-MWCNTs) have wider band gaps compared to 0.6% Nd-ZnO-MWCNTs, although narrower than that of pure ZnO. This observation is consistent with that made under the discussion on visible light absorptivity. This observation implies that both f-MWCNTs and Nd played specific roles in decreasing the band gap of ZnO and hence enhancing its visible light activity as there is a direct relationship between narrow photocatalyst band gap and high visible light activity [24].

3.6 Photocatalytic degradation test

The purpose of this study is to assess the capability of the synthesized ZnO, Nd-ZnO, and Nd-ZnO-MWCNTs photocatalysts to degrade organic pollutants in water. This aim has been achieved by applying the photocatalyst in the degradation of acid blue 40 dye in water under simulated solar light. The results of these analyses are shown in
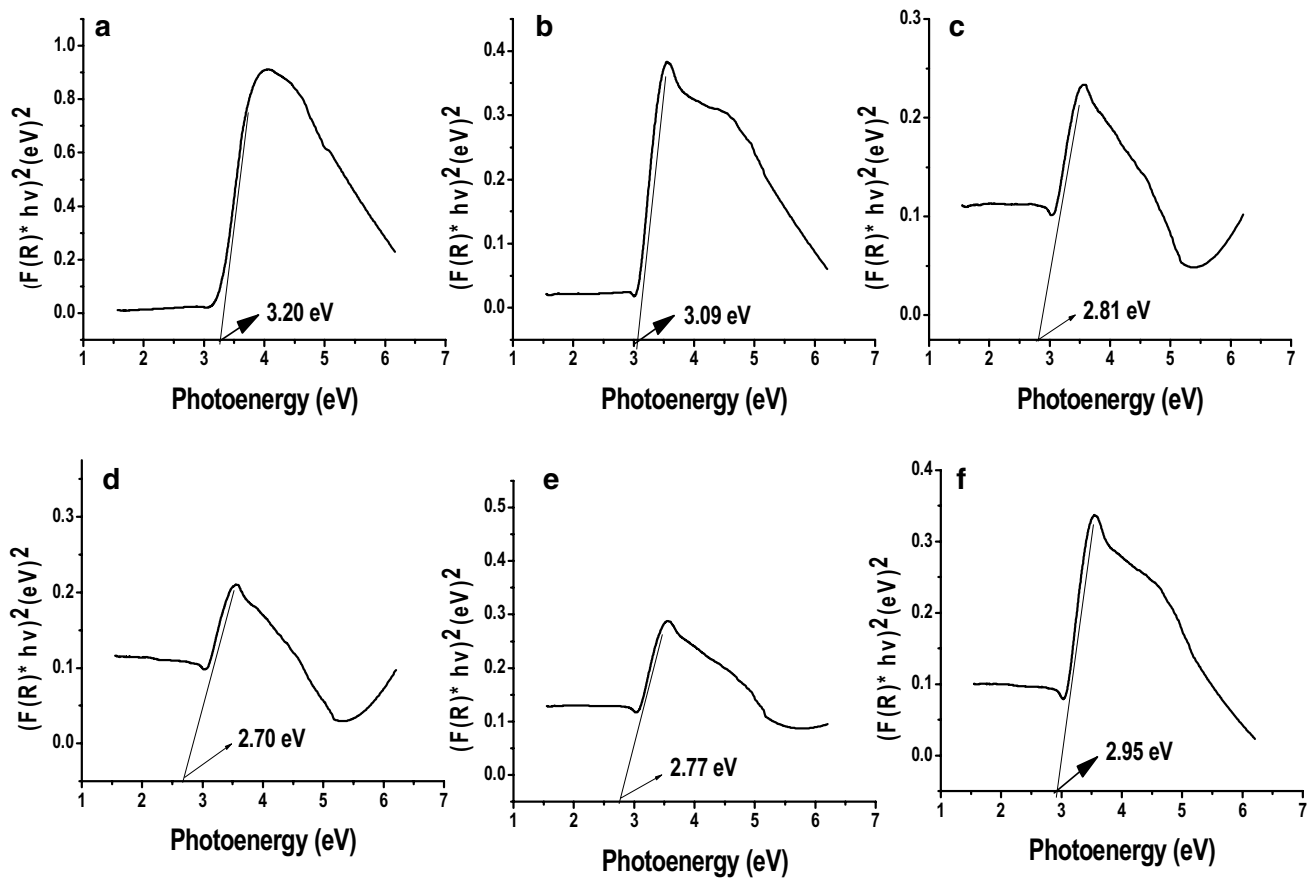
Fig. 5 Tauc plot for (**a**) ZnO, (**b**) ZnO-MWCNTs, (**c**) 0.3% Nd-ZnO-MWCNTs, (**d**) 0.6% Nd-ZnO-MWCNTs, (**e**) 1.0% Nd-ZnO-MWCNTs and (**f**) 2% Nd-ZnO-MWCNTs
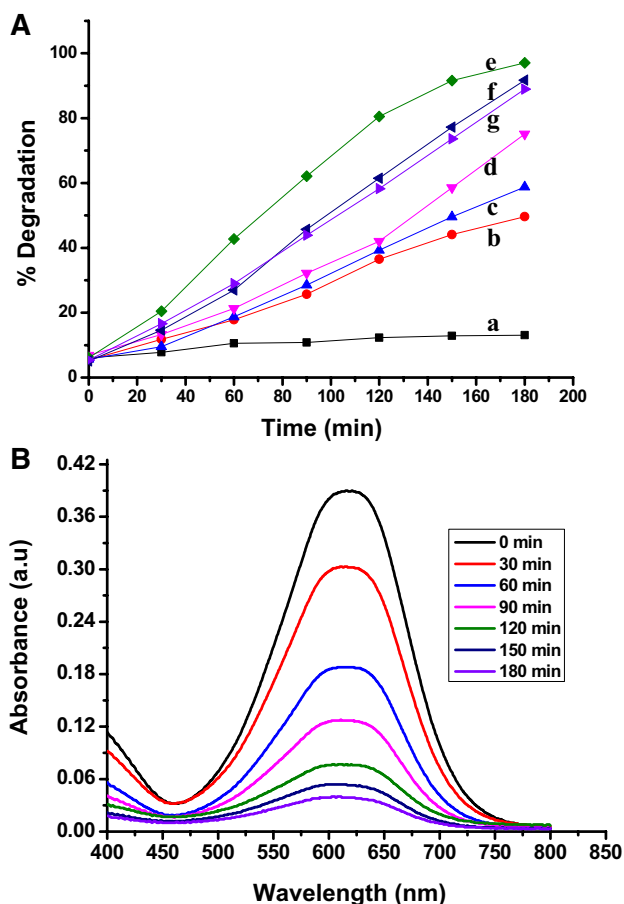
Fig. 6A and Table 1. According to the result, all the photocatalysts, except the bare ZnO, degraded the dye to various extents. The unmodified ZnO barely degraded the dye. 0.6% Nd-ZnO-MWCNTs displayed the highest degradation efficiency by degrading the dye to 99% within 180 min of visible light exposure. The increasing order of the efficiencies of the photocatalysts in the degradation of the dye is as follows: ZnO < ZnO-MWCNTs < 0.3% Nd-ZnO < 0.3% Nd-ZnO-MWCNTs < 0.2% Nd-ZnO-MWCNTs < 1.0% Nd-ZnO-MWCNTs < 0.6% Nd-ZnO-MWCNTs with their percent degradations presented in Table 1. The trend of the degradation efficiencies follows the observation made under visible light absorption and band gap analysis where 0.6% Nd-ZnO-MWCNTs possessed the least band gap and exhibited the highest visible light absorption; and thus, was expected to be the catalyst to degrade the dye with the highest efficiency. The result indicates that the introduction of MWCNTs and Nd played significant roles in the efficiency of the catalyst. Both Nd and MWCNTs decreased the band gap of the catalyst with the subsequent improvement in its visible light absorptivity. Rare earth metal dopants are also known to reduce recombination rates of

photogenerated electrons and holes through the creation of impurity states [25] thereby augmenting the photocatalytic activity of the resultant catalyst. MWCNTs, apart from possessing a large surface area, is known to act as a photosensitizer [26]. As a result, it enhanced the photoabsorptivity and pollutant adsorption tendency of the catalyst resulting in its improved performance. It can, therefore, be said that the synergistic effect of both Nd and MWCNTs caused the remarkable effectiveness of the catalyst in the degradation of the dye.

The change in the UV–visible spectrum of the dye with increasing light exposure time throughout the degradation process using 0.6% Nd-ZnO-MWCNTs is shown in Fig. 6B. A steady decline in the typical absorption band of the dye at 610 nm with increasing time is observed suggesting the steady degradation of the dye with time until 180 min when it was about 99% degraded.

3.7 The kinetics of photodegradation

The kinetics of the dye degradation by the catalysts was studied. To achieve this, the normalized dye
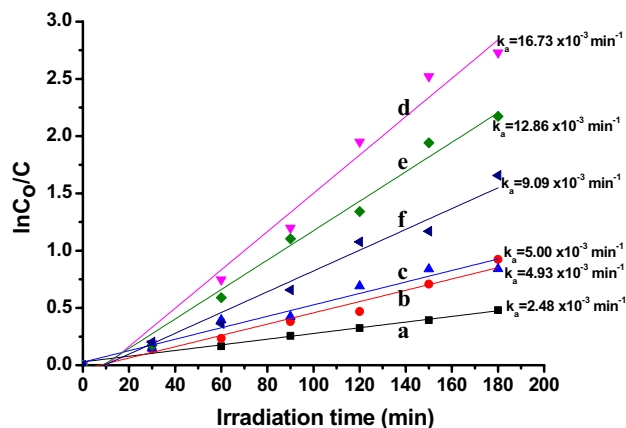
Fig. 7 Kinetics of acid blue 40 dye photodegradation of (**a**) ZnO, (**b**) ZnO-MWCNTs, (**c**) 0.3% Nd-ZnO-MWCNTs, (**d**) 0.6% Nd-ZnO-MWC-NTs (**e**) 1.0% Nd-ZnO-MWCNTs and (**f**) 2% Nd-ZnO-MWCNTs
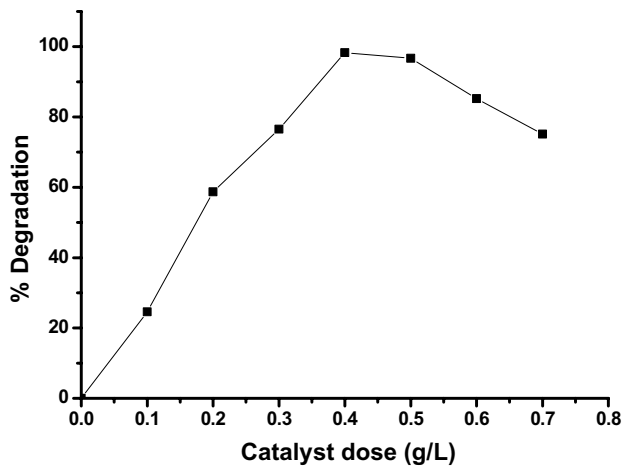
3.8 Effect of catalyst dose on dye degradation

It is always necessary to determine the optimum catalyst dose in any photolytic degradation process in order to avoid wasting the catalyst and ensure efficient photons absorption. The effect of catalyst dose on dye degradation was performed with catalyst masses ranging from 0.1–0.7 g/L with the results presented in Fig. 8. According to the result, the photodegradation process increased with increasing catalyst dose from 0.1 mg/L up to 0.4 g/L where 99% of the dye was degraded within 180 min. However, the dye degradation efficiency decreased with catalyst doses higher than 0.4 g/L. Thus, 0.4 g/L is the optimum catalyst dose for effective degradation. The increase in the mass of the catalyst resulted in a corresponding increase in available active surface area for the dye molecules adsorption resulting in enhanced dye degradation. Beyond 0.4 g/L, the solution becomes turbid. The turbid solution scattered the incident light, thus reduced light penetration

Fig. 6 A Acid blue 40 degradation efficiency of (**a**) ZnO, (**b**) ZnO-MWCNTs, (**c**) 0.3% Nd-ZnO, (**d**) 0.3% Nd-ZnO-MWCNTs, (**e**) 0.6% Nd-ZnO-MWCNTs, (**f**) 1.0% Nd-ZnO-MWCNTs and (**g**) 2% Nd-ZnO-MWCNTs; and (**B**) Photodegradation profile of acid blue 40 using 0.6%Nd-ZnO-MWCNTs

concentration (C_o/C) was plotted again time (t) using Langmuir-Hinselwood's first-order reaction expression shown in Eq. 3, with K being the apparent rate constants. C_o and C represent the initial and final dye concentrations respectively after degradation within time t.

$$\ln \frac{C_o}{C} = kt \qquad (3)$$

The result of this analysis, which is depicted in Fig. 7, attests to the superior photocatalytic degradation capability of 0.6% Nd-ZnO-MWCNTs nanocomposite compare to the others. This catalyst degraded the dye at a rate of 16.73×10^{-3} per min. This rate is about sevenfold higher than that of the least effective catalyst (bare ZnO) which is $2.48\ 10^{-3}$ per min. The performance of all the catalysts in terms of their rate of degradation of the dye is shown in Table 2.

Table 2 Band gap, percentage degradation, and kinetics of degradation after exposure to visible-light radiation for 180 min

Sample	Band gap (eV)	Degradation (%)	$K_a \times 10^{-3}$ (min^{-1})
ZnO	3.20	13.0	2.48
ZnO-MWCNTs	3.09	49.6	4.93
0.3% Nd-ZnO MWCNTs	2.81	75.1	5.00
0.6% Nd-ZnO-MWCNTs	2.70	99.0	16.73
1.0% Nd-ZnO-MWCNTs	2.77	91.7	12.86
2.0% Nd-ZnO-MWCNTs	2.95	88.9	9.09

Fig. 8 Effect of catalyst dose on dye degradation efficiency using 0.6% Nd-ZnO-MWCNTs
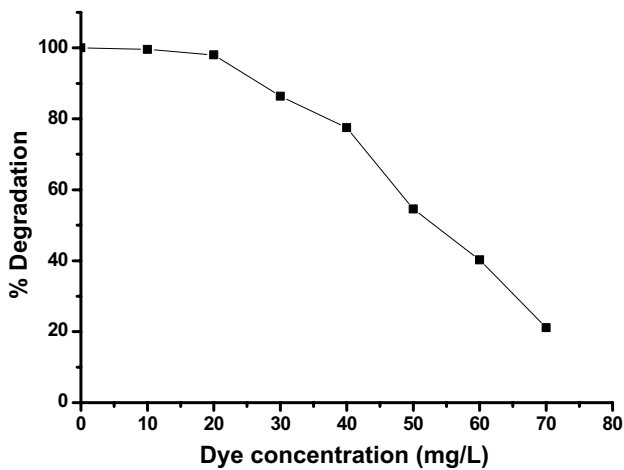
Fig. 9 Effect of dye concentration on degradation efficiency using 0.6% Nd-ZnO-MWCNTs

into the solution [27] leading to diminished degradation efficiency.

3.9 Influence of initial dye concentration

The result of the analysis on the influence of the dye concentration ranging from 5–70 mg/L on degradation efficiency is presented in Fig. 9. A consistent decrease in degradation efficiency was observed with increasing dye concentration. With increasing dye concentration, a corresponding increase of the dye molecule adsorption on the surface of the catalyst occurs. This reduces the available surface area of the catalyst for hydroxy radical generation leading to the reduction in degradation efficiency. Also, with increasing dye concentration, the colour

of the solution becomes deeper and hinders efficient light penetration of the solution. The dye molecules absorb a greater portion of the incident light and prevent it from reaching the catalyst's surface to encourage the generation of hydroxyl radicals [28]. This result agrees with the observation made by Chanu et al. [29].

3.10 Degradation of eosin Y dye

The capacity of the catalyst in degrading another dye apart from acid blue 40 was established by applying it in the degradation of eosin Y dye as well. As can be observed in Fig. 10, 0.6% Nd-ZnO-MWCNTs is also effective against eosin Y dye with about 80% efficiency. This catalyst can, therefore, be regarded as a potential effective photocatalyst against the degradation of a variety of organic dyes in water.

3.11 Catalyst reusability study

One of the important parameters to be considered in choosing an appropriate catalyst for photocatalytic application is its reusability. Subsequently, the reusability of 0.6% Nd-ZnO-MWCNTs (the most efficient photocatalyst) has been studied. The catalyst was recovered after each degradation cycle through centrifugation, regenerated with dilute HCl, washed copiously with deionized, dried and reused for 6 successive cycles. The results, according to Fig. 11, shows that the catalyst can be recycled and reused for 5 consecutive times before it begins to lose its efficiency. The first five cycles of the catalyst's reusability exhibit efficiencies ranging from 98 to 95% within the 180 min irradiation time. A noticeable reduction in its reusability was identified after the fifth cycle resulting in 76% degradation efficiency. The result shows that the catalyst can be efficiently recycled and reused for 5 consecutive times for the degradation of dyes in water.
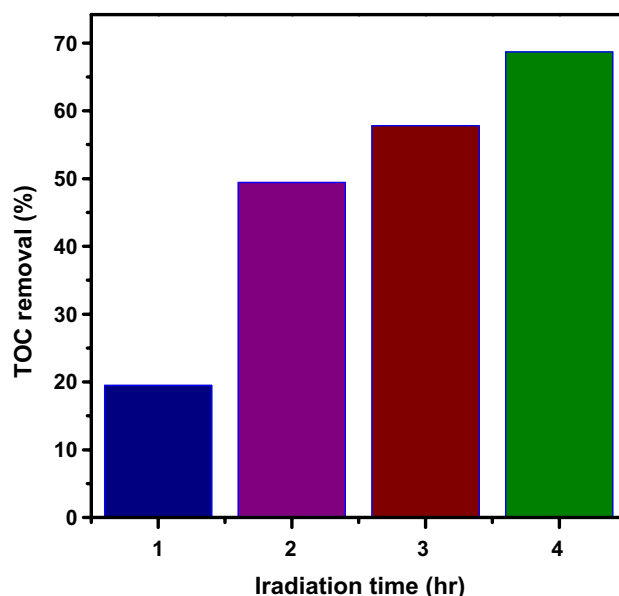
3.12 Total organic carbon (TOC) analysis

TOC analysis of the treated water was performed to assess the degree to which the dye (acid blue 40) was mineralized since the disappearance of dye colour alone cannot be used as a measure of its complete mineralization. The analysis was done with 0.6% Nd-ZnO-MWCNTs using the Fusion UV/persulfate TOC analyser at different time intervals up to 4 h at the optimum conditions. The result of this analysis (Fig. 12) revealed an appreciable level of mineralization of the dye (69%) after 4 h. The result also points out the potential conversion of the dye into other intermediate forms and signifies that degradation of the dye beyond 4 h may lead to complete mineralization.

Fig. 10 Photodegradation profile of Eosin Y dye using 0.6%Nd-ZnO-MWCNTs
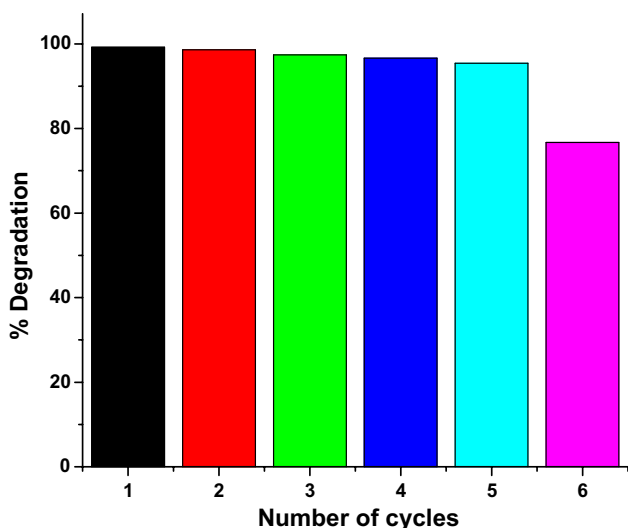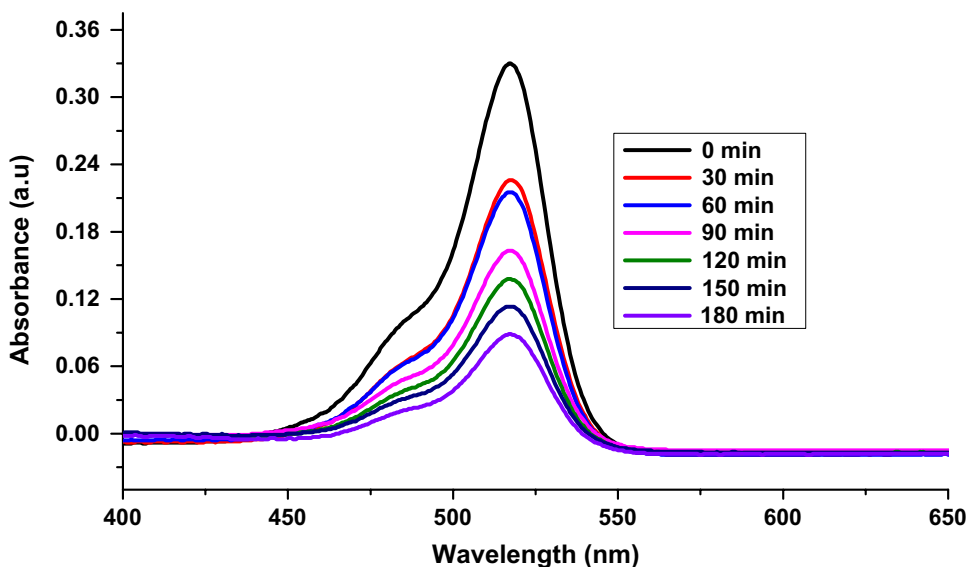
Fig. 11 Acid blue 40 dye photodegradation efficiency of recycled 0.6% Nd-ZnO-MWCNTs nanocomposite

Fig. 12 Total organic carbon analysis of the degraded dye solution using 0.6% Nd-ZnO-MWCNTs

3.13 Comparison of photodegradation effectiveness of the as-synthesized 0.6% Nd-ZnO-MWCNTs nanocomposite with other published results
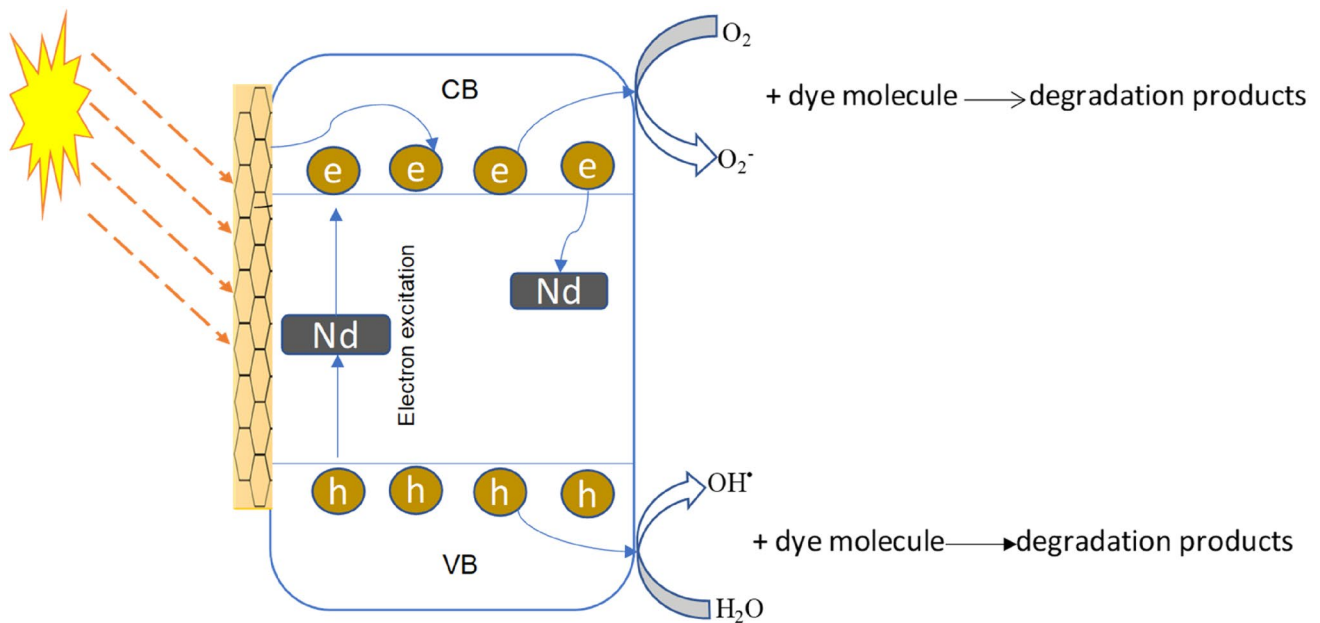
The photocatalytic degradation performance of 0.6% Nd-ZnO-MWCNTs photocatalyst has been compared with other published work involving ZnO based photocatalysts for the degradation of dyes in water under visible light irradiation (Table 3). The table clearly shows that 0.6% Nd-ZnO-MWCNTs photocatalyst is more efficient than the other ZnO based photocatalysts for dyes degradation in water.

3.14 Proposed photocatalytic degradation mechanism of the Nd-ZnO-MWCNTs Photocatalyst

The possible mechanism of photocatalysis is shown in Fig. 13. Upon visible light irradiation, excitation of electrons from the valence band (VB) to the conduction band (CB) of ZnO occurs leading to the creation of holes (h^+) in the VB and electrons (e^-) in the conduction band (CB). The h^+ in the VB oxidizes the dye molecules and further reacts with water molecules to generate

Table 3 Comparison of photodegradation efficiency of 0.6% Nd-ZnO-MWCNTs catalyst to other ZnO based photocatalysts for the degradation of dyes in water

Catalysts	Dyes	Reaction time (min)	Illumination type	Efficiency (%)	References
ZrO_2–ZnO	Methylene blue	180	UV	97	[30]
ZnO	Methyl orange	120	UV	91	[25]
La-ZnO	Methyl orange	180	UV	85.6	[26]
GO/ZnO	Basic fuchsin	180	UV	92.5	[30]
N-ZnO	Methylene blue	180	UV–Vis	98.6	[31]
ZnO-SnS	Rhodamine	180	UV–Vis	95.0	[32]
Nd-ZnO	Acid blue 40	180	UV–Vis	99	Current study
Nd-ZnO	Eosin Y	180	UV–Vis	80.0	Current study

Fig. 13 Proposed visible-light-induced photocatalytic degradation mechanism of the dye by the Nd-doped ZnO-MWCNTs photocatalyst

hydroxyl radicals ($OH^{\cdot}$). The CB electrons also react with dissolved oxygen species to form superoxide radicals ($O_2^{-\cdot}$). The $OH^{\cdot}$ and $O_2^{-\cdot}$ induced redox reactions, leading to the complete mineralization of the dyes. The Nd-doped ZnO-MWCNTs composites showed better photocatalytic performance due to the increase in the number of impurity energy levels between the CB and VB which helps for the generation of more $e^{-} – h^{+}$ pairs, decrease recombination of photogenerated holes and electrons in ZnO. The empty orbitals of Nd acted as a sink for electrons which prevented electron–hole recombination [12] while the MWCNTs released electrons onto the CB of the ZnO leading to the enhanced photodegradation performance of the composite [13].

4 Conclusion

The unmodified, and Nd and MWCNTs modified ZnO nanocomposites have been successfully synthesized using the co-precipitation method and confirmed by TEM, XRD, and FTIR analyses. TEM analysis showed that the catalysts are spherical and were well distributed on the MWCNTs. XRD analysis revealed a wurtzite crystalline phase of ZnO. Modification with Nd and MWCNTs decreased the band gap of ZnO from 3.2 to 2.7 eV resulting it enhanced visible light absorption. 0.6% Nd was identified to be the optimum Nd concentration beyond which the band gap, visible light activity and

photodegradation efficiency of the catalyst were hampered. All the modified catalysts degraded the dyes under visible light irradiation. 0.6% Nd-ZnO-MWCNTs exhibited the highest acid blue 40 dye degradation efficiency of 99% while the bare ZnO exhibited only 13% efficiency. 0.4 g/L was identified as the optimum catalyst dose for effective degradation. TOC analysis revealed 69% mineralization after 4 h indicating that degradation beyond 4 h may lead to complete mineralization. Reusability study confirms the catalyst to be stable and can be reused for 5 consecutive times without significantly losing its efficiency. The excellent degradation efficiency of the catalyst is attributed mainly to the band gap reduction with the subsequent improvement in visible light activity due to the synergistic effects of both Nd and MWCNTs.

Compliance with ethical standards

Conflict of interest The authors declare no conflict of interest in the publication of this article and have all agreed on its publication in this journal.

References

1. Ahmed T et al (2016) Water-related impacts of climate change on agriculture and subsequently on public health: a review for generalists with particular reference to Pakistan. Int J Environ Res Public Health 13(11):1051

2. Qu X, Alvarez PJ, Li Q (2013) Applications of nanotechnology in water and wastewater treatment. Water Res 47(12):3931–3946

3. Paraschiv D, Tudor C, Petrariu R (2015) The textile industry and sustainable development: a holt-winters forecasting investigation for the Eastern European area. Sustainability 7(2):1280–1291

4. Sarkar S et al (2017) Degradation of synthetic azo dyes of textile industry: a sustainable approach using microbial enzymes. Water Conserv Sci Eng 2(4):121–131

5. Crini G, Lichtfouse E (2019) Advantages and disadvantages of techniques used for wastewater treatment. Environ Chem Lett 17(1):145–155

6. Teh CY et al (2016) Recent advancement of coagulation–flocculation and its application in wastewater treatment. Ind Eng Chem Res 55(16):4363–4389

7. Tobaldi D et al (2015) Nitrogen-modified nano-titania: true phase composition, microstructure and visible-light induced photocatalytic NOx abatement. J Solid State Chem 231:87–100

8. Kumar SG, Rao KK (2017) Comparison of modification strategies towards enhanced charge carrier separation and photocatalytic degradation activity of metal oxide semiconductors (TiO_2, WO_3 and ZnO). Appl Surf Sci 391:124–148

9. Obeid MM et al (2019) Unraveling the effect of Gd doping on the structural, optical, and magnetic properties of ZnO based diluted magnetic semiconductor nanorods. RSC Adv 9(57):33207–33221

10. Pesci FM et al (2013) Efficient suppression of electron–hole recombination in oxygen-deficient hydrogen-treated TiO_2 nanowires for photoelectrochemical water splitting. J Phys Chem C 117(48):25837–25844

11. Liu S, Guo E, Yin L (2012) Tailored visible-light driven anatase TiO_2 photocatalysts based on controllable metal ion doping and ordered mesoporous structure. J Mater Chem 22(11):5031–5041

12. Oppong SO-B et al (2016) Photocatalytic degradation of indigo carmine using Nd-doped TiO_2-decorated graphene oxide nanocomposites. J Sol–Gel Sci Technol 80(1):38–49

13. Anku WW et al (2016) Cobalt doped ZrO_2 decorated multi-walled carbon nanotube: a promising nanocatalyst for photodegradation of indigo carmine and eosin Y dyes. Prog Nat Sci Mater Int 26(4):354–361

14. Da Dalt S, Alves AK, Bergmann CP (2016) Preparation and performance of tio2-zno/cnt hetero-nanostructures applied to photodegradation of organic dye. Mater Res 19(6):1372–1375

15. Ramoraswi NO, Ndungu PG (2015) Photo-catalytic properties of TiO_2 supported on MWCNTs, SBA-15 and silica-coated MWCNTs nanocomposites. Nanoscale Res Lett 10(1):427

16. Gangu KK, Maddila S, Jonnalagadda SB (2019) A review on novel composites of MWCNTs mediated semiconducting materials as photocatalysts in water treatment. Sci Total Environ 646:1398–1412

17. Singh A (2010) Synthesis, characterization, electrical and sensing properties of ZnO nanoparticles. Adv Powder Technol 21(6):609–613

18. Ravi K et al (2018) ZnO/RGO nanocomposite via hydrothermal route for photocatalytic degradation of dyes in presence of visible light. Int J Chem Stud 6(6):20–26

19. Baharudin L et al (2020) CO oxidation and the inhibition effects of carboxyl-modification and copper clusters on multi-walled carbon nanotubes. Appl Catal B 262:118265

20. Luna-Flores A et al (2019) Improvement of the photocatalytic activity of ZnO/Burkeite heterostructure prepared by combustion method. Catalysts 9(10):817

21. Jaramillo-Páez C, Navío JA, Hidalgo M (2018) Silver-modified ZnO highly UV-photoactive. J Photochem Photobiol, A 356:112–122

22. Wang J et al (2012) Oxygen vacancy induced band-gap narrowing and enhanced visible light photocatalytic activity of ZnO. ACS Appl Mater Interfaces 4(8):4024–4030

23. Bingham S, Daoud WA (2011) Recent advances in making nano-sized TiO_2 visible-light active through rare-earth metal doping. J Mater Chem 21(7):2041–2050

24. Gao T et al (2015) Enhanced visible-light-driven photoactivities of single-walled carbon nanotubes coated with N doped TiO_2 nanoparticles. RSC Adv 5(37):28973–28979

25. Munshi GH, Ibrahim AM, Al-Harbi LM (2018) Inspired preparation of zinc oxide nanocatalyst and the photocatalytic activity in the treatment of methyl orange dye and paraquat herbicide. Int J Photoenergy 2018

26. Suwanboon S et al (2013) Optical and photocatalytic properties of La-doped ZnO nanoparticles prepared via precipitation and mechanical milling method. Ceram Int 39(3):2811–2819

27. Reza KM, Kurny A, Gulshan F (2017) Parameters affecting the photocatalytic degradation of dyes using TiO_2: a review. Appl Water Sci 7(4):1569–1578

28. Saggioro EM et al (2011) Use of titanium dioxide photocatalysis on the remediation of model textile wastewaters containing azo dyes. Molecules 16(12):10370–10386

29. Chanu LA et al (2019) Effect of operational parameters on the photocatalytic degradation of Methylene blue dye solution using manganese doped ZnO nanoparticles. Results Phys 12:1230–1237

30. Durmus Z, Kurt BZ, Durmus A (2019) Synthesis and characterization of graphene oxide/zinc oxide (GO/ZnO) nanocomposite and its utilization for photocatalytic degradation of basic Fuchsin dye. ChemistrySelect 4(1):271–278

31. Prabakaran E, Pillay K (2019) Synthesis of N-doped ZnO nanoparticles with cabbage morphology as a catalyst for the efficient photocatalytic degradation of methylene blue under UV and visible light. RSC Adv 9(13):7509–7535

32. Wang L et al (2017) 3D porous ZnO–SnS p–n heterojunction for visible light driven photocatalysis. Phys Chem Chem Phys 19(25):16576–16585